Molten metal *closo*-borate solvates

Kasper T. Møller,[1,2]* Mark Paskevicius,[1,2] Jacob G. Andreasen,[1] Junqiao Lee,[3] Nigel Chen-Tan,[2] Jacob Overgaard,[1] SeyedHosein Payandeh,[1] Debbie S. Silvester,[3] Craig E. Buckley,[2] Torben R. Jensen.[1]*

[1]*Interdisciplinary Nanoscience Center (iNANO) and Department of Chemistry, University of Aarhus, DK-8000 Aarhus, Denmark*

[2]*Department of Imaging and Applied Physics, Fuels and Energy Technology Institute, Curtin University, GPO Box U1987, Perth 6845, WA, Australia.*

[3] *Curtin Institute for Functional Molecules and Interfaces, School of Molecular and Life Sciences, Curtin University, GPO Box U1987, Perth 6845, WA, Australia.*

*Corresponding Authors: Kasper T. Møller, kasper.moller@curtin.edu.au and Torben R. Jensen, trj@chem.au.dk

Experimental

Sample preparation

As purchased $Li_2B_{12}H_{12}·4H_2O$ (Katchem) was dehydrated at T = 225 °C in dynamic vacuum for 16 hours. The dehydrated $Li_2B_{12}H_{12}$ was confirmed by NMR to be pure, see Figure S1. Subsequently, the product, $Li_2B_{12}H_{12}$, was transferred to round bottom flasks closed with a septum. Five different solvents were used in this study, *i.e.* tetrahydrofuran (THF), acetonitrile (ACN), triethylamine (TEA), dimethylsulfide (DMS), and diethylether (DEE). Solvent was added to $Li_2B_{12}H_{12}$ (65 mL g^{-1} $Li_2B_{12}H_{12}$) and the mixture was stirred for 15 minutes. Finally, the solvent was removed *in vacuo* at T = 0 °C to prevent decomposition of potential $Li_2B_{12}H_{12}$ adducts.

The $Li_2B_{12}H_{12}$ was observed to be fully soluble in DMS, TEA and ACN. All handling of samples were performed in an argon filled glovebox ($p(O_2, H_2O)$ < 1 ppm) or using standard Schlenk techniques to maintain an inert atmosphere.

Melt infiltration of $Li_2B_{12}H_{12}·x$ACN ($1 < x < 8$) was conducted into mesostructured silica, *i.e.* SBA-15 (SiO_2, Sigma-Aldrich, 99%, 8 nm pores) by heating a physical mixture of 0.07205 g SBA-15 (dried under dynamic vacuum for 14 hours at 300 °C) and 0.30099 g $Li_2B_{12}H_{12}$-xACN to 200 °C ($\Delta T/\Delta t$ = 5 °C/min) in an argon atmosphere, before increasing the temperature to 260 °C under dynamic vacuum and keeping isothermal conditions for 10 hours. The SBA-15 scaffold was chosen to directly compare results to a previous study.[1]

Single crystals of $Li_2B_{12}H_{12}·8$ACN and $Li_2B_{12}H_{12}·6$THF were grown by solvent evaporation. A few mg of $Li_2B_{12}H_{12}$ was dispensed in the respective solvent and in the THF experiment, excess $Li_2B_{12}H_{12}$ was left to settle and the top layer of solvent was decanted to another container. Subsequently, the solvent was left to evaporate at room temperature (RT) and single crystals precipitated.

Single-crystal X-ray diffraction, Structure Solution, and Refinement

X-ray diffraction on the $Li_2B_{12}H_{12}$·8ACN and $Li_2B_{12}H_{12}$·6THF crystals was carried out using an Oxford Diffraction Supernova diffractometer equipped with a microfocus MoK_α X-ray source (λ = 0.71073 Å) and an Oxford Cryosystems Cryostream 700 that allowed the crystal temperature to be kept at 100 K. The crystals were loaded into inert oil in an argon-filled glove box, before being mounted on the diffractometer using a goniometer head. Data on $Li_2B_{12}H_{12}$·6THF were collected to a resolution of 0.74 Å with an average redundancy of 2.7 and an agreement factor *R*(int) of 2.3%, and on $Li_2B_{12}H_{12}$·8ACN to 0.73 Å with an average redundancy of 4.5 and *R*(int) of 4.9%. The structures were solved using SHELXT[2] and refined using SHELXL.[3] CCDC 1882904 ($Li_2B_{12}H_{12}$·6THF) and 1882905 ($Li_2B_{12}H_{12}$·8ACN) contains the supplementary crystallographic data for this paper. This data can be obtained free of charge via www.ccdc.cam.ac.uk.

Powder X-ray Diffraction

PXD data of as-prepared samples were measured on a Rigaku Smart Lab diffractometer using a Cu source and a convergent beam incident optics (Cu $K_{\alpha1}$ radiation, λ = 1.54056 Å, Cu $K_{\alpha2}$ radiation, λ = 1.54439 Å). Data were collected in the 2θ-range 8 to 60° at 3°/min using a Rigaku D/tex detector. All samples were mounted in an argon-filled glovebox in 0.5 mm glass capillaries sealed with glue.

In Situ Synchrotron Radiation Powder X-ray Diffraction

High resolution, *in situ* temperature-variable SR-PXD data was collected at beamline B01A at the ESRF, Grenoble, France on a wide-angle position sensitive detector (PSD) based on Mythen-2 Si strip modules, λ = 0.82585 Å. The powdered samples were packed in borosilicate capillaries (i.d. 0.5 mm) in an argon-filled glovebox ($p(O_2, H_2O)$ < 1 ppm). Subsequently, the samples were heated from room temperature to 300 °C ($\Delta T/\Delta t$ = 5 °C min^{-1}), while being rotated during data acquisition. The temperature was calibrated from a NaCl standard.[4]

Fourier Transformed Infrared Spectroscopy

Fourier Transformed Infrared Spectroscopy was performed on a PerkinElmer Spectrum 100 spectrometer. Data were measured between 4000 and 650 cm^{-1} with a spectral resolution of 4 cm^{-1}. A total of 32 scans were collected and averaged per sample. The instrument does not allow for inert atmosphere, thus the samples were briefly exposed to air upon mounting.

Thermal Analysis

Thermogravimetric analysis (TGA) and differential scanning calorimetry (DSC) of the five solvated samples were collected simultaneously using a PerkinElmer STA 6000 apparatus. The samples (approx. 10 mg) were placed in Al_2O_3 crucibles under a protective argon atmosphere in a glovebox and heated from 35 to 400 °C ($\Delta T/\Delta t$ = 5 °C/min) in an argon flow of 40 mL/min.

Temperature Programmed Photographic Analysis

A pellet of $Li_2B_{12}H_{12}{\cdot}x$ACN (~10 mg) was pressed and sealed in a glass tube under an argon atmosphere and placed in a custom-made aluminium heating block [5]. The sample was heated from RT to 150 °C ($\Delta T/\Delta t$ = 4 °C/min) while photos of the sample were collected every six seconds. The $Li_2B_{12}H_{12}{\cdot}x$Solv. (Solv. = DEE, THF, TEA, DMS) were heated from RT to 400 °C ($\Delta T/\Delta t$ = 5 °C/min)

Small angle X-ray Scattering

Small angle X-ray scattering (SAXS) was performed on a Bruker Nanostar instrument equipped with a galium metaljet source (λ = 1.34 Å) and a VÅNTEC-2000 2-D detector. Samples were powders pressed between tape, measured under vacuum at room temperature. Data were background corrected and transformed onto an absolute intensity scale using a glassy carbon calibration standard.[6,7] Scattering contrast was calculated using the X-ray scattering length density for SiO_2 (22.45 x 10^{10} cm^{-2}) and $Li_2B_{12}H_{12}$ (10.03 x 10^{10} cm^{-2}). The pore infiltration level is calculated from the ratio between theoretical and experimentally measured values of the (100) peak intensity, *i.e.* theoretically $\Delta\rho^2$(fully loaded scaffold) / $\Delta\rho^2$(empty scaffold) = 0.306 whilst this ratio was experimentally determined to be 0.341, hence a loading of 90% was achieved.

Scanning Electron Microscopy

Scanning electron microscopy (SEM) was conducted using a Zeiss Neon 40EsB equipped with a field emission gun. The SEM images were collected using an accelerating voltage of 5 kV, an apperture size of 30 µm, and a working distance of 4 mm. SEM samples were prepared by dispersing powdered samples upon a pin type SEM mount (12 mm diameter) and coated with a 10 µm thick platinum layer.

Electrochemical Impedance Spectoscopy

Electrochemical impedance spectroscopy (EIS) was performed on pelletised powder ($Li_2B_{12}H_{12}$-SBA15) using a ZIVE SP1 electrochemical workstation. Powders were pressed into pellets (6 mm diameter, 3 mm thickness) at 1 tonne (346 MPa) sandwiched between gold foil (0.1 mm) and sealed within an air tight 'Swagelok-type' teflon cell with 316 stainless steel electrodes. Temperature was controlled with a tube furnace from room temperature to 200 °C and monitored by a K-type thermocouple 5 mm from the pellet. EIS was conducted at 100 mV from 0.01 Hz to 1 MHz and the intercept of the semi-circle on the Nyquist plot was used to calculate ion conductivity, as described earlier.[8]

EIS experiments on $Li_2B_{12}H_{12}$-*x*Solv. were carried out on platinium interdigitated array microelectrodes (ED-IDA6-Pt, MicruX, Oviedo, Spain). A reservoir (ca. 3 mm tall) was constructed with silicone (Selleys, New South Wales, Australia) and allowed to cure overnight. Wires were soldered onto the leads of the IDA6-Pt to allow interfacing with the potentiostat. The cell constant of the IDA was calibrated at 21.2 ± 0.1 °C using 0.100 ± 0.001 M $KCl_{(aq)}$ solution, and found to be at 96.7 ± 0.2 m^{-1}. Two samples of dried $Li_2B_{12}H_{12}$ were separately dissolved in THF and ACN under argon. The silicon reservoir on the IDA6-Pt was then filled with the respective solutions of $Li_2B_{12}H_{12}$ within a glass-cell under a constant nitrogen stream, and held at 55 °C on a heating plate (RCT basic, IKA-Werke, Staufen im Breisgau, Germany). The solvents were allowed to dry, and the process was repeated until the reservoir was almost completely filled by the powder material after solvent

volatilisation. The plate-temperature was then increased to 65 °C for another 30 minutes to allow any residual uncoordinated solvents to volatilise off. The $Li_2B_{12}H_{12}$·*solv* in the reservoir was then gently compacted and covered with a small cut piece of glass coverslip before being completely sealed with silicone. The base of the IDA6-Pt was placed in thermal contact with the heating plate using a heatsink compound (R001, ChemTools, NSW, Australia), and the setup was then covered with a a double layer of aluminium foil, internally padded with cotton wool (for insulation), and weighed down with a watchglass. A schematic of the setup is provided in Figure S1. The EIS measurements were carried out with an EIS capable potentiostat (PGSTAT302N with FRA32M module, Metrohm Utrecht, the Netherlands) at an amplitude of 50 mV and scanned between 0.1 Hz to 1 MHz. The samples were kept at temperature for > 30 minutes before conducting the EIS measurement. The Nyquist plots were similarly analysed as discussed above.

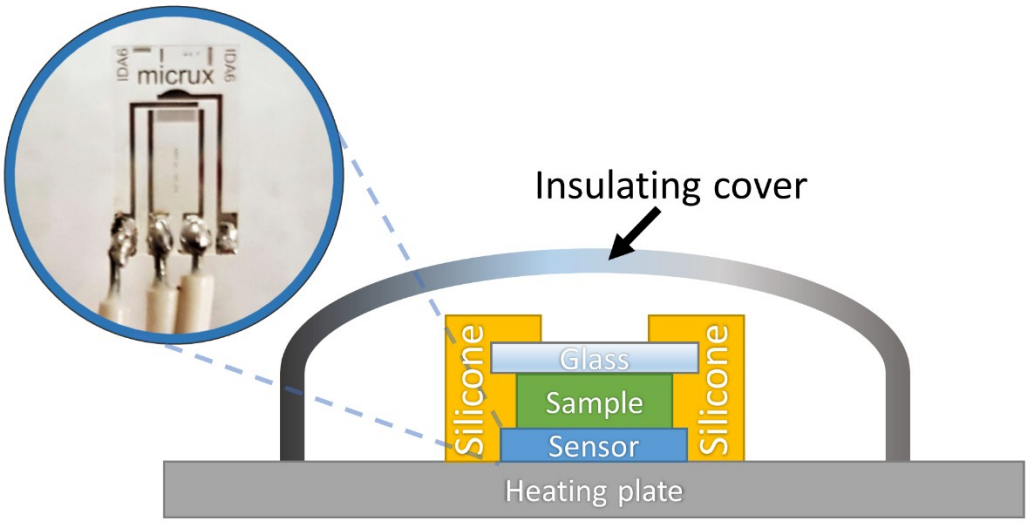

Figure S1. Schematic of the EIS setup used to measure the $Li_2B_{12}H_{12}$-*x*Solv samples.

Table S1. Overview of samples made and products obtained. None of the products have previously been reported in literature.

Compound	**Solvent**	**Product**
$Li_2B_{12}H_{12}$	DEE	$Li_2B_{12}H_{12}{\cdot}x$DEE*
	ACN	$Li_2B_{12}H_{12}{\cdot}$8ACN
	THF	$Li_2B_{12}H_{12}{\cdot}$6THF
	TEA	$Li_2B_{12}H_{12}{\cdot}x$TEA*
	DMS	$Li_2B_{12}H_{12}{\cdot}x$DMS*

*$0.5 < x < 8$

Table S2. Basic crystallographic information on the crystal structures of $Li_2B_{12}H_{12}{\cdot}$8ACN and $Li_2B_{12}H_{12}{\cdot}$6THF.

	$Li_2B_{12}H_{12}{\cdot}$8ACN	**$Li_2B_{12}H_{12}{\cdot}$6THF**
Crystal system	Tetragonal	Monoclinic
Space group (no.)	$P4_12_12$ (92)	$C2/c$ (15)
***a* (Å)**	10.0374(4)	14.7037(4)
***b* (Å)**	10.0374(4)	14.1409(3)
***c* (Å)**	31.778(2)	18.2503
***β* (°)**	-	111.270(3)
***V* (Å^3)**	3201.6(3)	3536.19(14)
Z	8	8
Data collection *T* (K)	100	100
Wavelength, *λ* (Å)	0.7107	0.7107

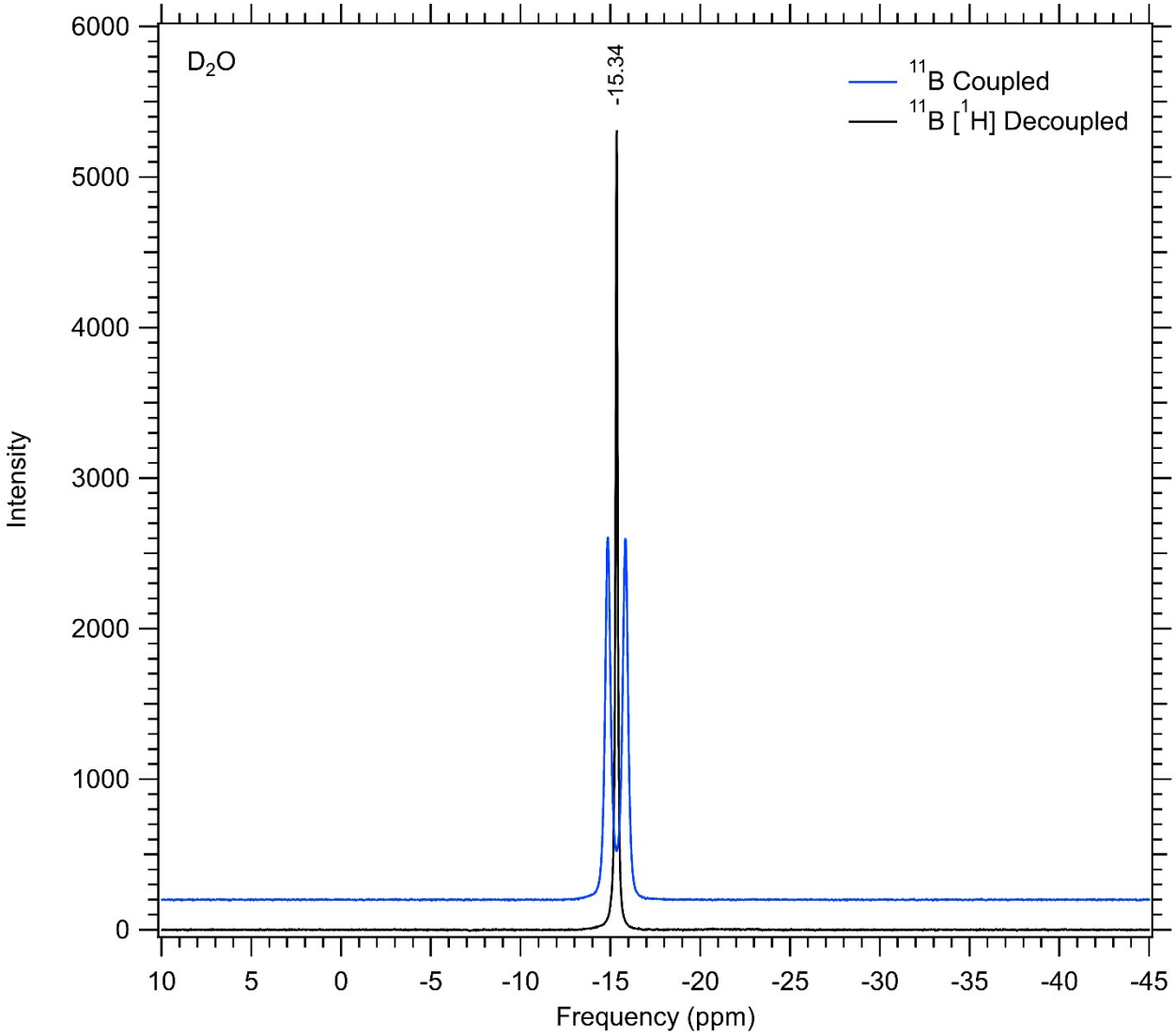

Figure S2. NMR of the starting reagent $Li_2B_{12}H_{12}$ showing only one ^{11}B signal assigned to $Li_2B_{12}H_{12}$.

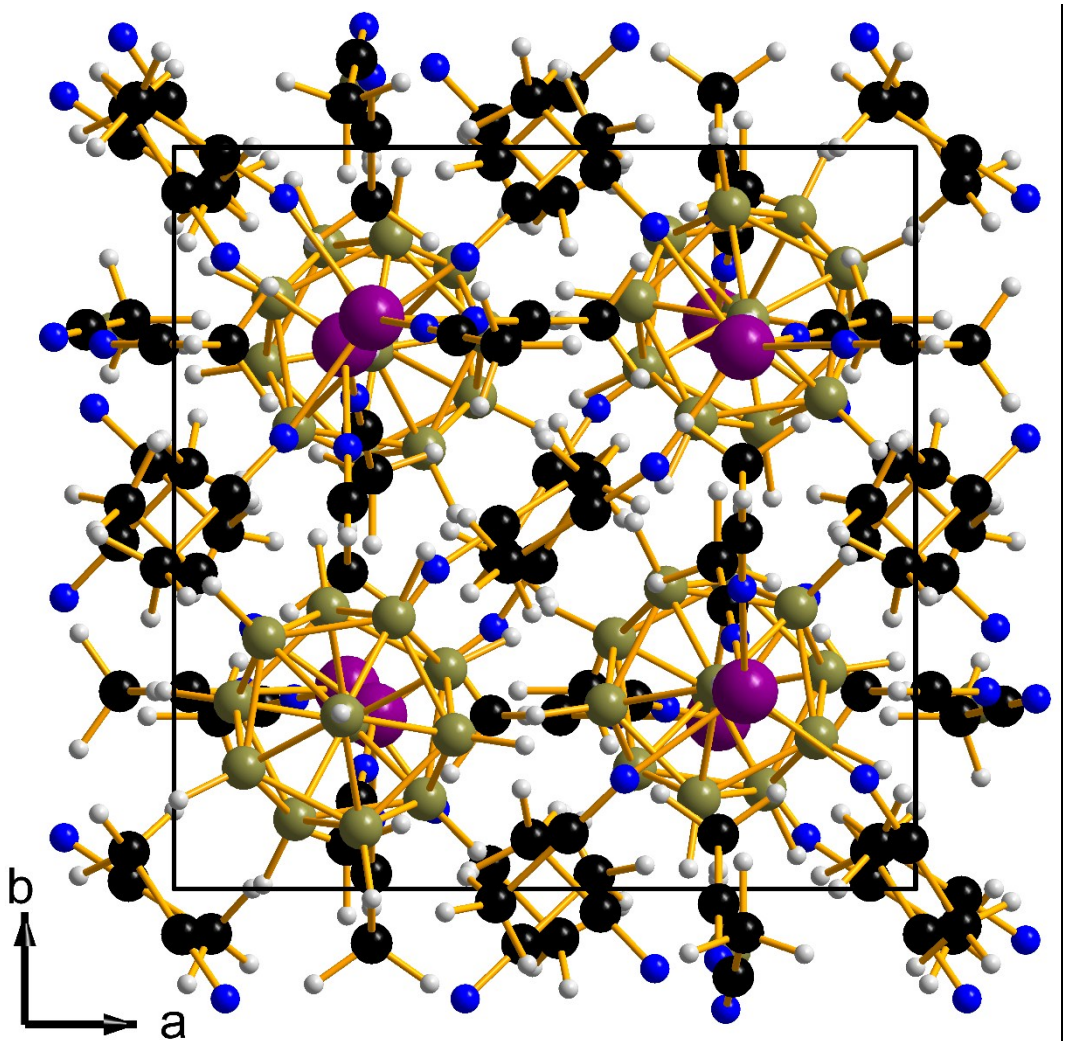

Figure S3. Crystal structure of $Li_2B_{12}H_{12}$·8ACN (spacegroup $P4_12_12$), $a = b = 10.0374(4)$ Å; $c = 31.778(2)$ Å.

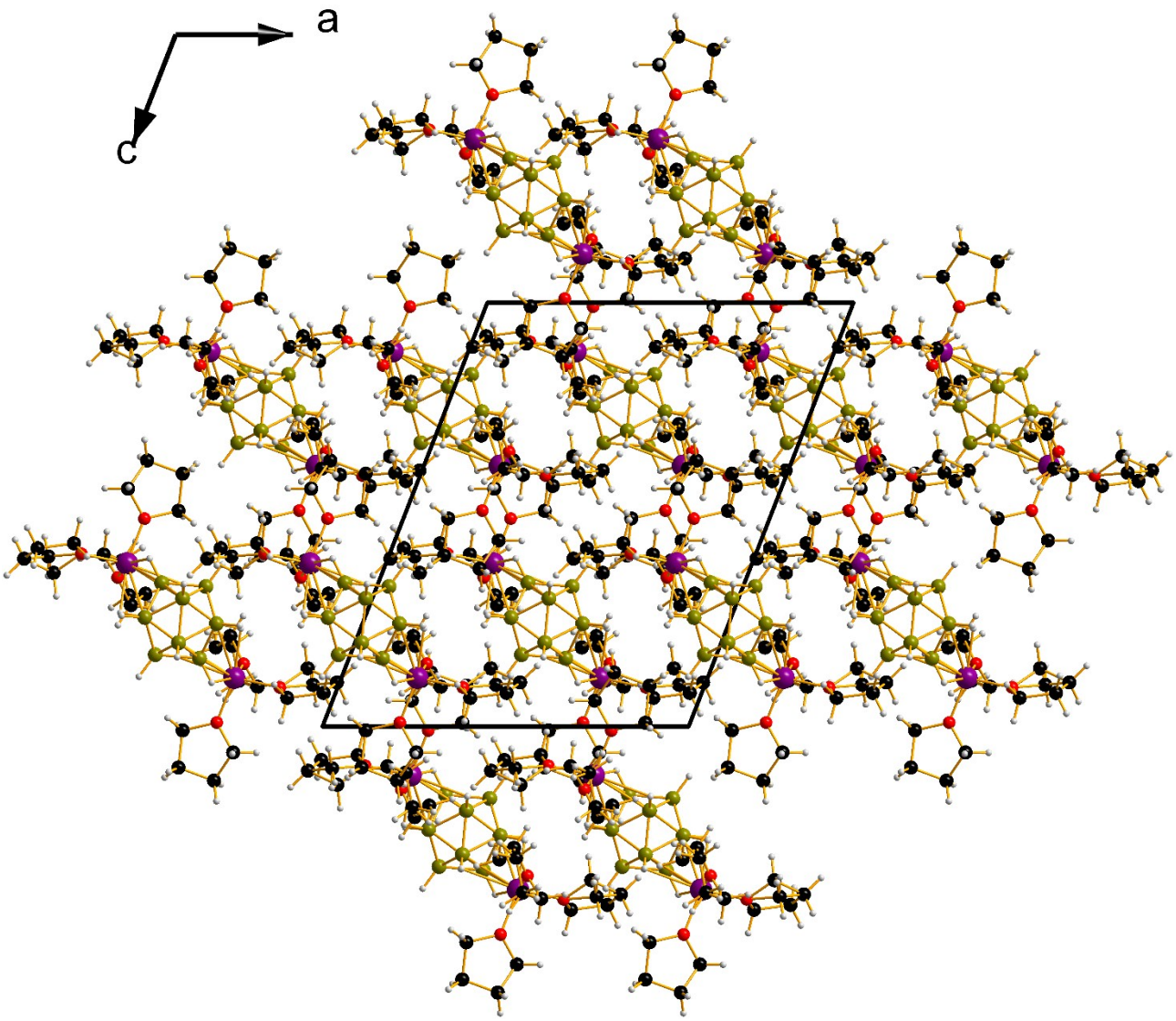

Figure S4. Crystal structure of) $Li_2B_{12}H_{12}$·6THF (spacegroup *C*2/*c*), a = 14.7037(4) Å; b = 14.1409(3) Å; c = 18.2503(4) Å; β = 111.270(3)°. One carbon atom in the THF ring has occupancy in two different positions. In the figure, one of the positions has been omitted for simplicity.

In Situ Synchrotron Radiation Powder X-ray Diffraction

All samples were analysed by SR-PXD. The data shows the complexity of the changes in crystal structure as the compounds release the solvent and also provides evidence of melting as the Bragg reflections suddenly disappear upon heating and reappear upon cooling. Crystallographic indexing of the intermediate solvate structures did not provide satisfying unit cells, and thus crystal structure solution was abandoned.

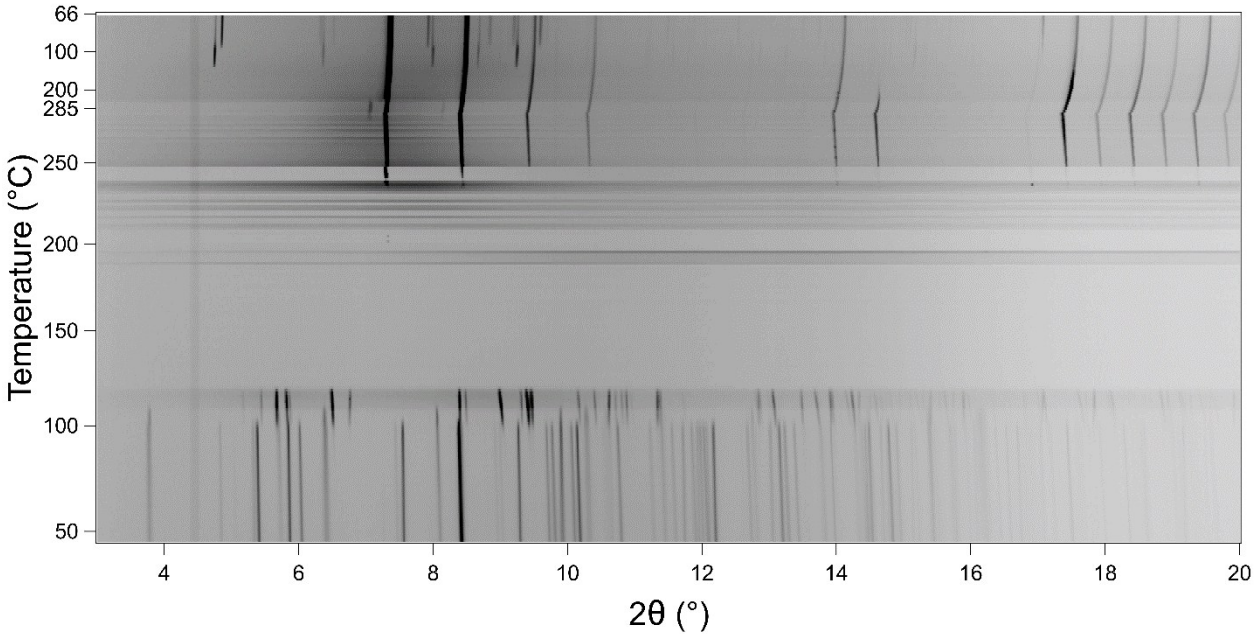

Figure S5. *In situ* SR-PXD of $Li_2B_{12}H_{12}{\cdot}x$ACN heated from room temperature to 300 °C ($\Delta T/\Delta t$ = 5 °C min^{-1}), λ = 0.7129 Å, p(Ar) = 1 bar.

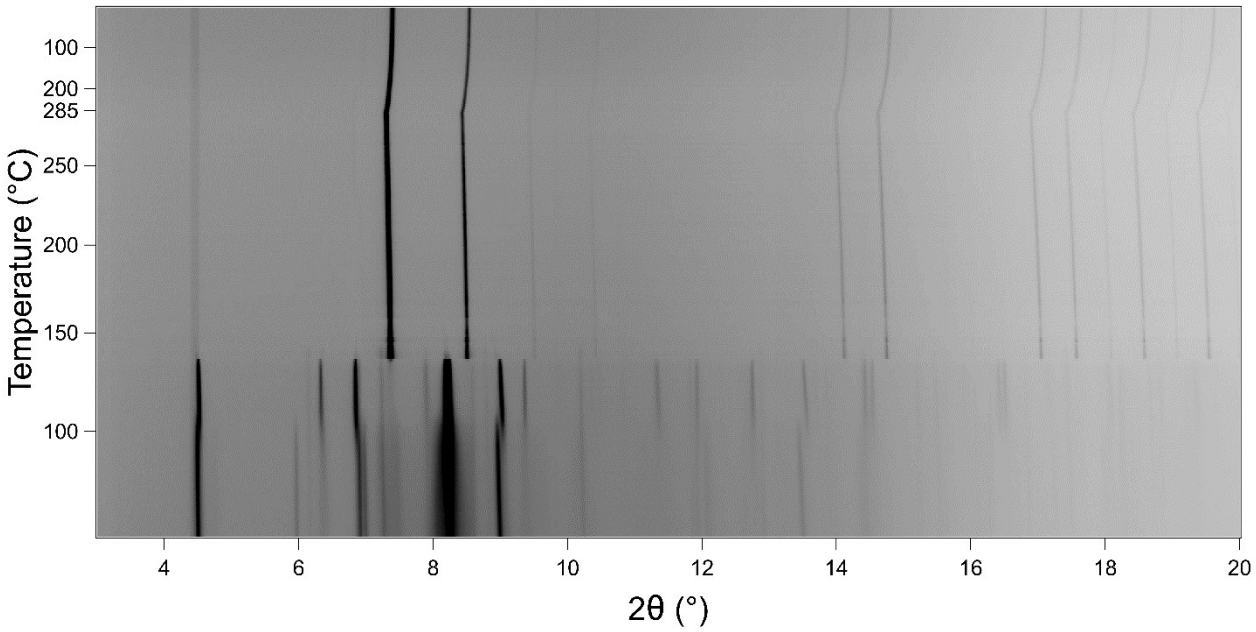

Figure S6. *In situ* SR-PXD of $Li_2B_{12}H_{12}$·*x*DEE heated from room temperature to 300 °C ($\Delta T/\Delta t$ = 5 °C min^{-1}), λ = 0.7129 Å, *p*(Ar) = 1 bar.

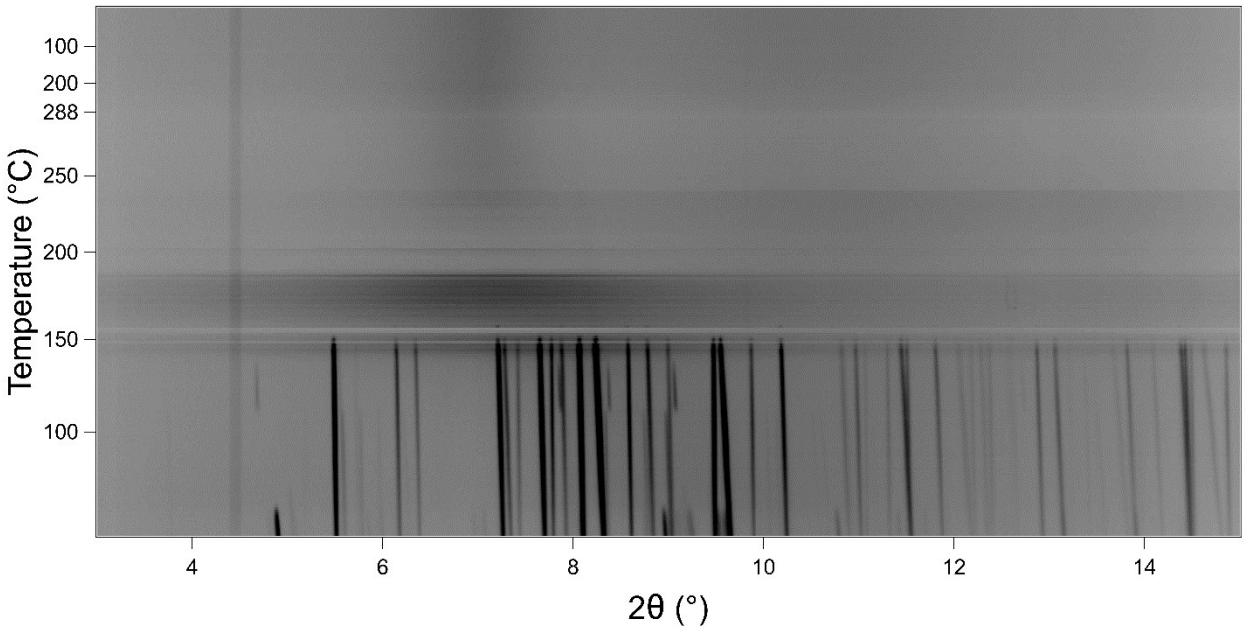

Figure S7. *In situ* SR-PXD of $Li_2B_{12}H_{12}$·*x*DMS heated from room temperature to 300 °C ($\Delta T/\Delta t$ = 5 °C min^{-1}), λ = 0.7129 Å, *p*(Ar) = 1 bar.

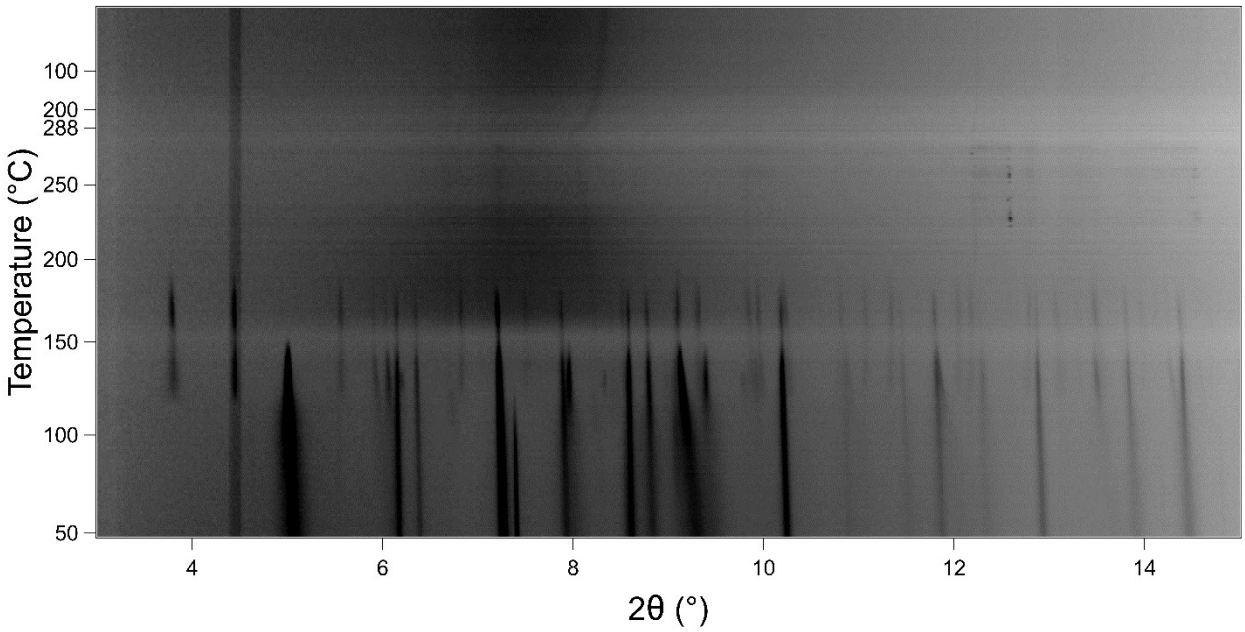

Figure S8. *In situ* SR-PXD of $Li_2B_{12}H_{12}$·*x*TEA heated from room temperature to 300 °C ($\Delta T/\Delta t$ = 5 °C min^{-1}), λ = 0.7129 Å, *p*(Ar) = 1 bar.

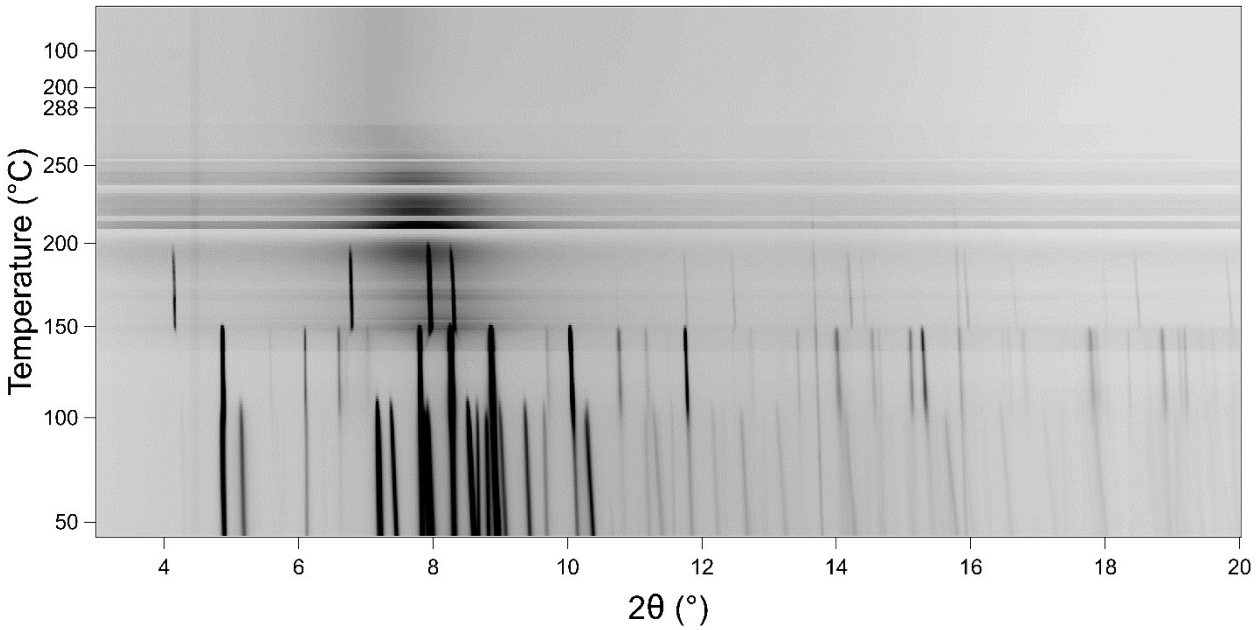

Figure S9. *In situ* SR-PXD of $Li_2B_{12}H_{12}$·*x*THF heated from room temperature to 300 °C ($\Delta T/\Delta t$ = 5 °C min^{-1}), λ = 0.7129 Å, *p*(Ar) = 1 bar.

Thermal Analysis

The thermogravimetric analysis of the $Li_2B_{12}H_{12}$·Solv. (Solv. = dimethylsulphide (DMS), diethyl ether (DEE), and triethyl amine (TEA)) is presented in Figure S10. The loss of DEE occurs in one step at ~100 °C resulting in a weight loss of 30 wt.%. The DMS sample show two distinct weight losses of 1.8 wt.% and 17 wt.% at 75 and 95 °C, respectively. Similarly, the TEA sample releases solvent in two distinct steps of 6 wt.% and 13 wt.% at 105 and 221 °C, respectively.

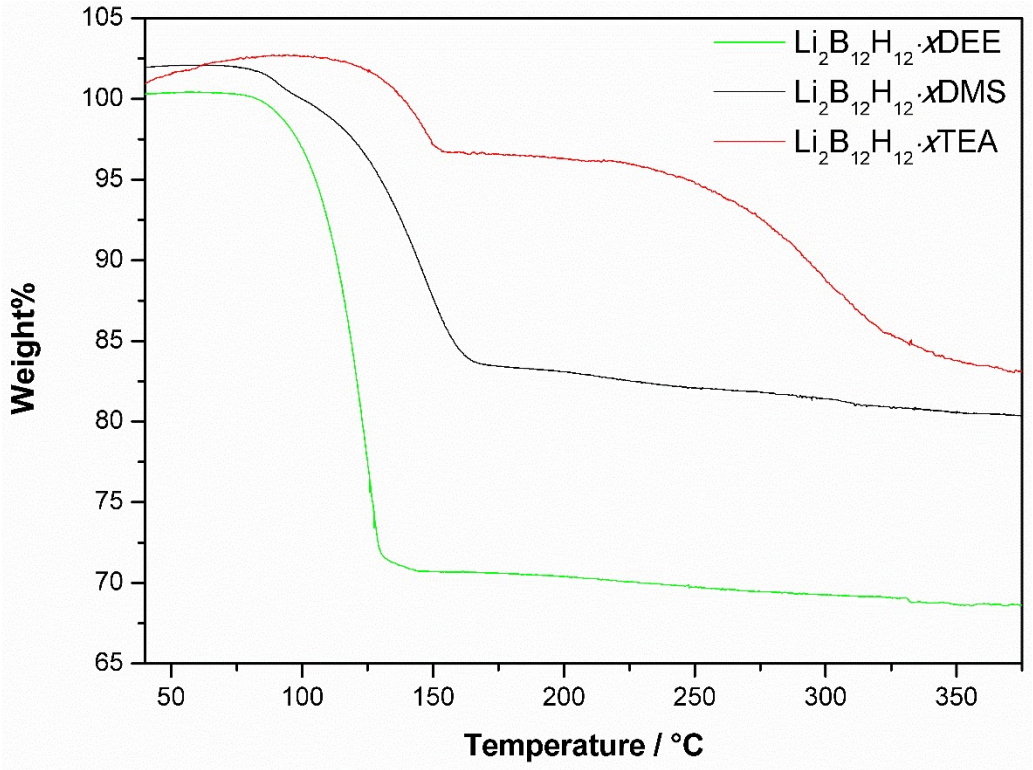

Figure S10. TGA of $Li_2B_{12}H_{12}$·*x*DEE, $Li_2B_{12}H_{12}$·*x*DMS, and $Li_2B_{12}H_{12}$·*x*TEA heated from RT to 400 °C ($\Delta T/\Delta t$ = 5 °C/min).

Temperature Programmed Photographic Analysis

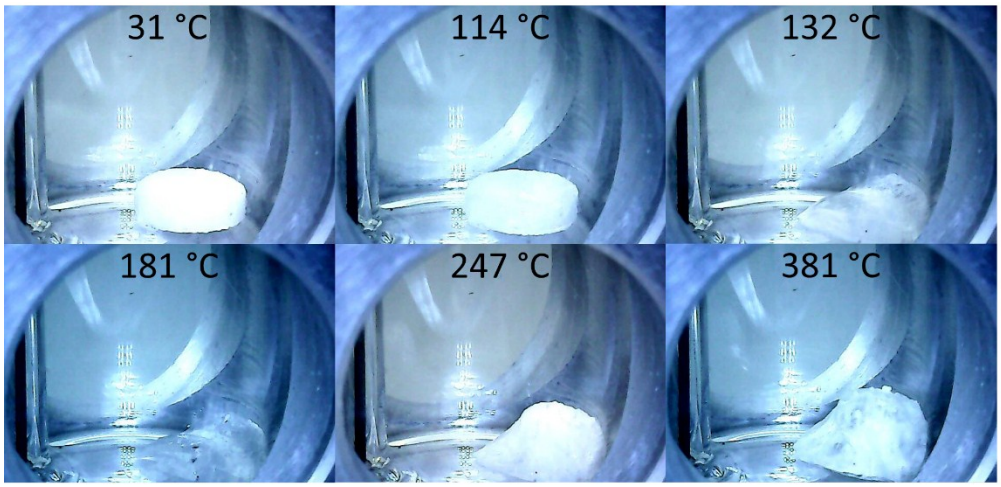

Figure S11. TPPA of $Li_2B_{12}H_{12}$·*x*ACN heated from *RT* to 400 °C ($\Delta T/\Delta t$ = 5 °C/min).

TPPA of $Li_2B_{12}H_{12}$·*x*DEE (Figure S12) reveals a gradual volume decrease of the sample as DEE is released. However, no major change is observed.

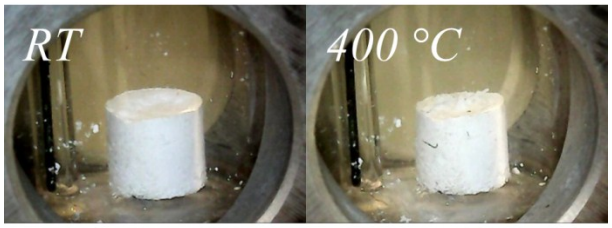

Figure S12. TPPA of $Li_2B_{12}H_{12}$·*x*DEE heated from *RT* to 400 °C ($\Delta T/\Delta t$ = 5 °C/min).

TPPA of $Li_2B_{12}H_{12}$·*x*DMS (Figure S13) reveals a similar behaviour to $Li_2B_{12}H_{12}$·*x*DEE as only a volume decrease of the sample is observed upon heating as DMS is released.

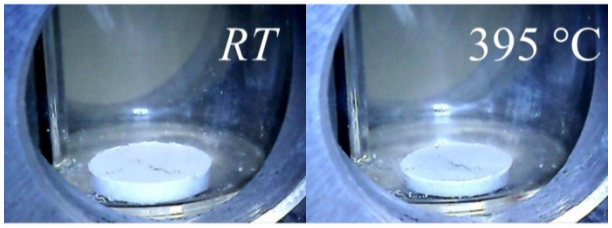

Figure S13. TPPA of $Li_2B_{12}H_{12}$·*x*DMS heated from *RT* to 395 °C ($\Delta T/\Delta t$ = 5 °C/min).

TPPA of $Li_2B_{12}H_{12}$·*x*TEA (Figure S14) shows a gradual colour change between 83 and 184 °C from white to light yellow, and the pellet almost looks wet. As the temperature reaches 280 °C a heavy foaming initiates, which continues to approximately 380 °C, *i.e.* the sample extensively expands upon heating. During foaming, the colour returns to white again.

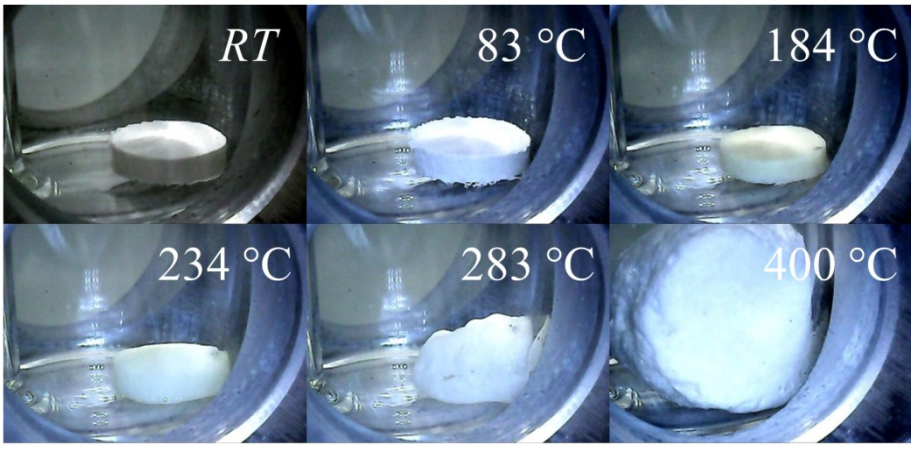

Figure S14. TPPA of $Li_2B_{12}H_{12}$·*x*TEA heated from *RT* to 400 °C ($\Delta T/\Delta t$ = 5 °C/min).

The $Li_2B_{12}H_{12}$·*x*THF sample (Figure S15) reveals a similar behaviour to $Li_2B_{12}H_{12}$·*x*ACN as the sample volume initially decreases. At $T \sim$ 120 °C the sample begins to melt and is completely molten at ~140 °C. Slightly above the melting temperature at $T >$ 155 °C, the liquid starts to 'boil' and as $T >$ 200 °C the sample begins to solidify, which is completed at ~220 °C. No further changes are observed up to 354 °C.

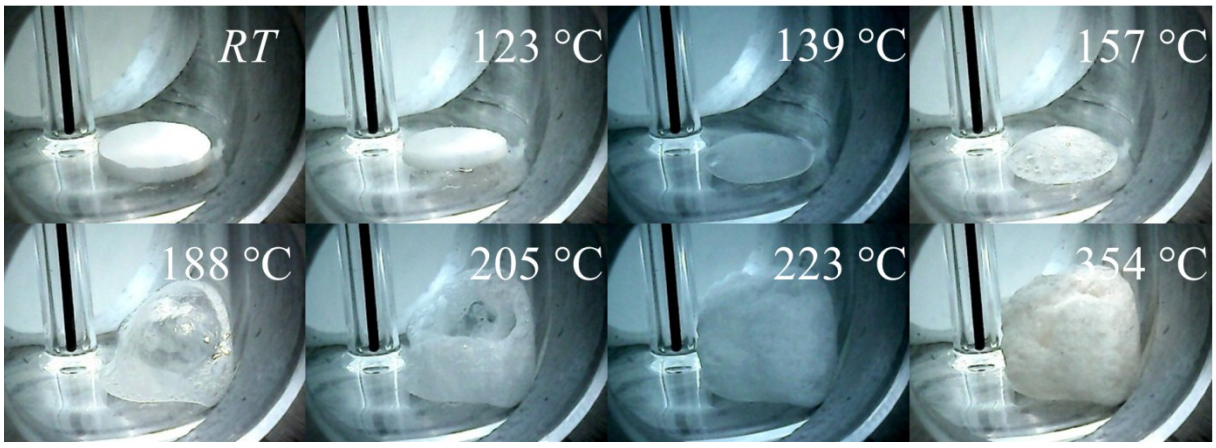

Figure S15. TPPA of $Li_2B_{12}H_{12}$·*x*THF heated from *RT* to 354 °C ($\Delta T/\Delta t$ = 5 °C/min).

Powder X-ray Diffraction

Powder X-ray diffraction of the dried SBA-15 reveals a bump indicating an amorphous compound, see Figure S16. The diffractogram of $Li_2B_{12}H_{12}$ and $Li_2B_{12}H_{12}{\cdot}x$ACN + SBA-15 are similar. However, a few reflections change intensity, which is assigned to a minor release of acetonitrile upon hand-grinding the physical mixture. Hence, a change from one phase to another is observed.

Finally, after melt infiltration of $Li_2B_{12}H_{12}{\cdot}x$ACN into the SBA-15 scaffold, only Bragg reflections from $Li_2B_{12}H_{12}$ are present.

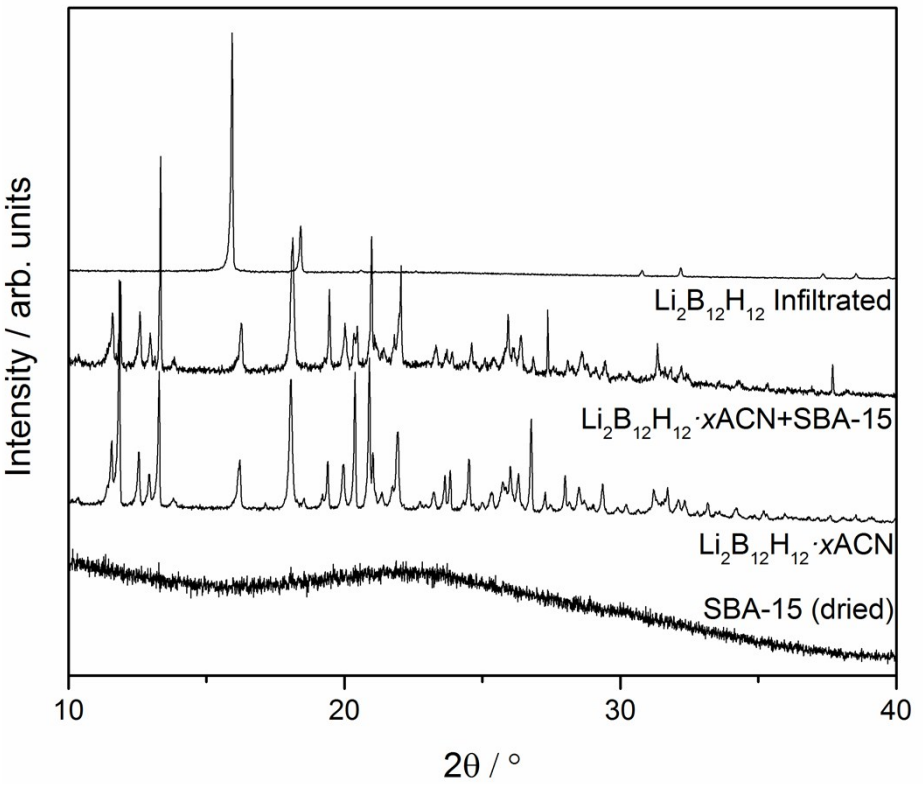

Figure S16. PXD data (λ = 1.54056 Å) comparing the dried SBA-15 with the $Li_2B_{12}H_{12}{\cdot}x$ACN, the physical mixture of $Li_2B_{12}H_{12}{\cdot}x$ACN-SBA-15, and the melt infiltrated sample. The infiltrated pattern shows that desolvated $Li_2B_{12}H_{12}$ is present.

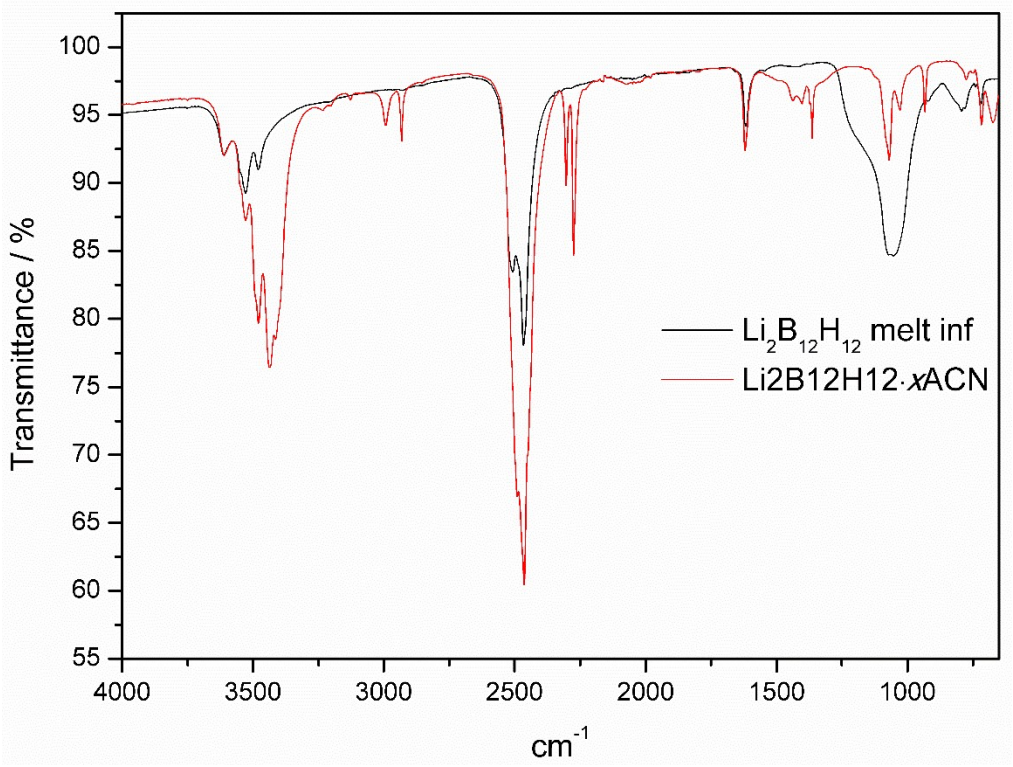

Figure S17. FT-IR data on $Li_2B_{12}H_{12}{\cdot}x$ACN and $Li_2B_{12}H_{12}$ melt infiltrated into SBA-15. The stretching and bending modes at 2992 (CH_3, ACN), 2932 (CH_3, ACN), 2304 ($Li^+\cdots$ACN complex), and 2275 cm^{-1} ($Li^+\cdots$ACN complex) originating from acetonitrile are no longer present after melt infiltration.[9] Also, two characteristic B—H stretching modes present at 2491 and 2465 cm^{-1} are assigned to $Li_2B_{12}H_{12}$. The stretching modes observed between 3600 – 3400 cm^{-1} are assigned to water and possibly CH_3C-N$\cdots$H-OH interactions.[10,11]

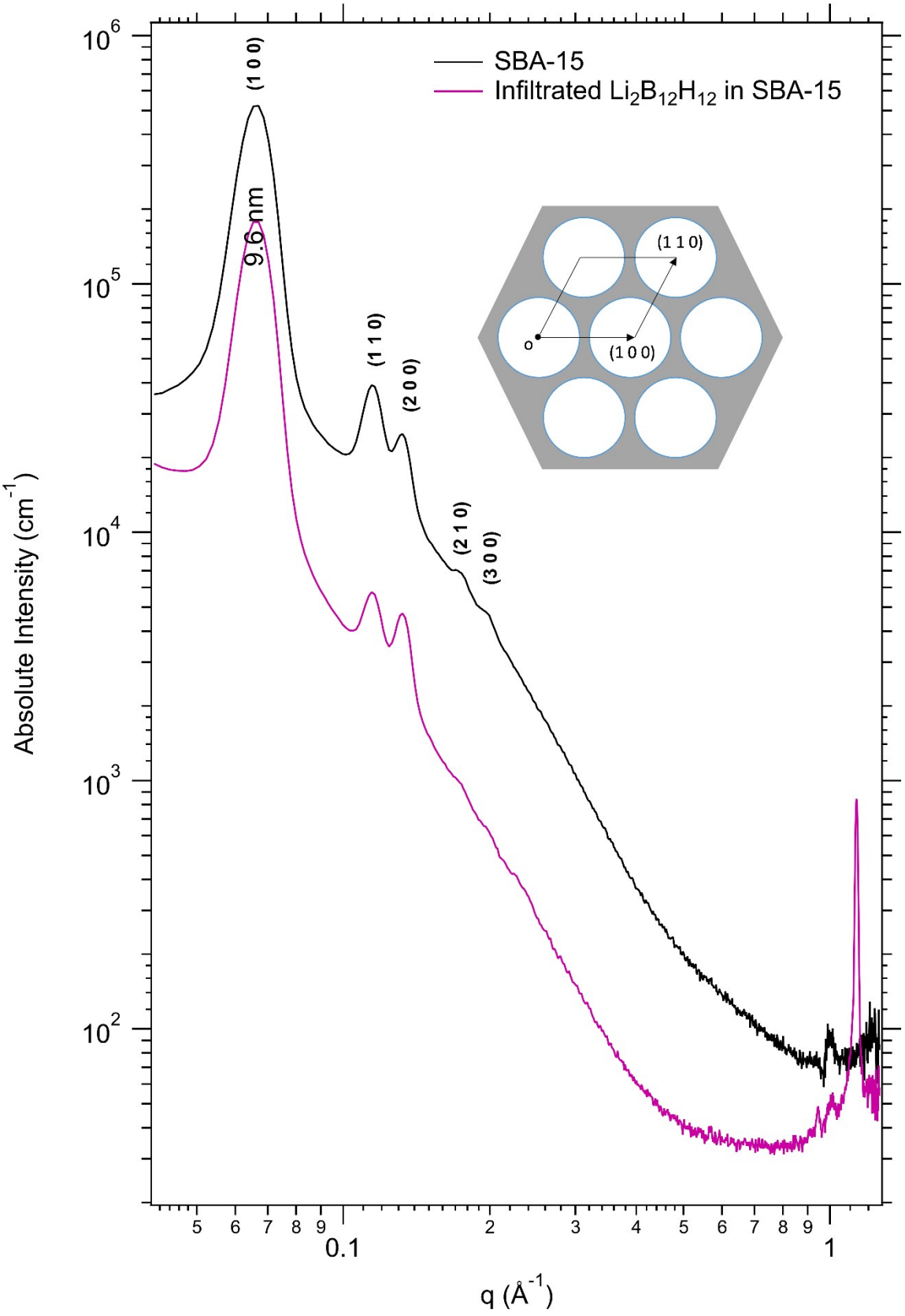

Figure S18. SAXS data on $Li_2B_{12}H_{12}$ melt infiltrated into SBA-15.

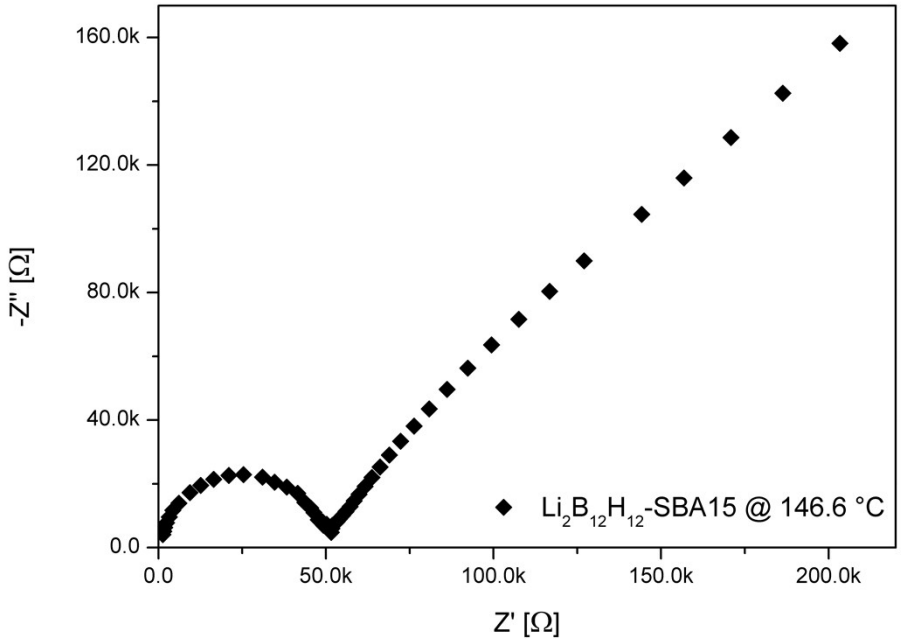

Figure S19. Nyquist plot of the pelletised $Li_2B_{12}H_{12}$-SBA15 sample at T = 146.6 °C.

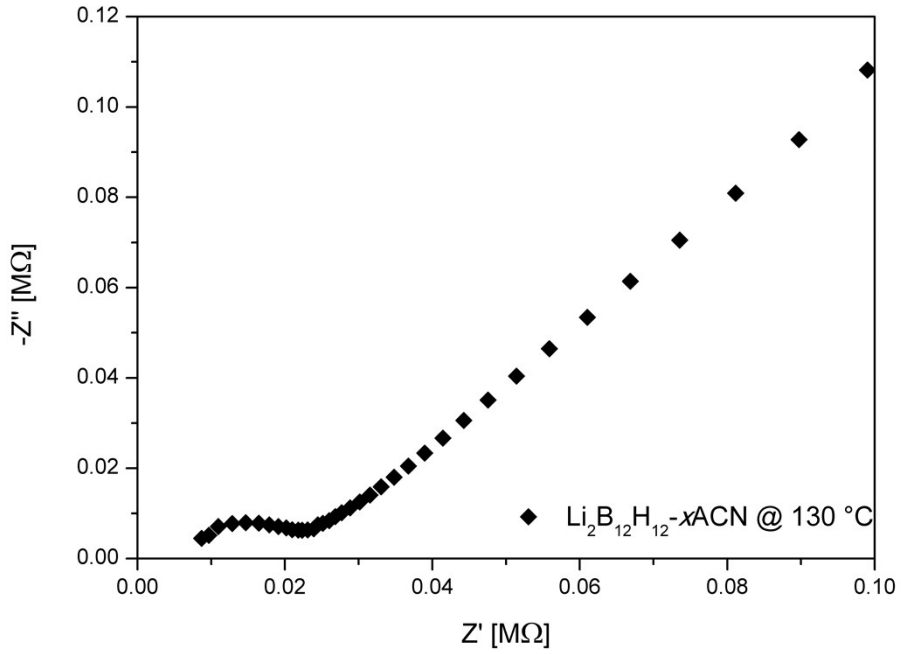

Figure S20. Nyquist plot of the molten $Li_2B_{12}H_{12}$-*x*ACN sample at T = 130 °C.

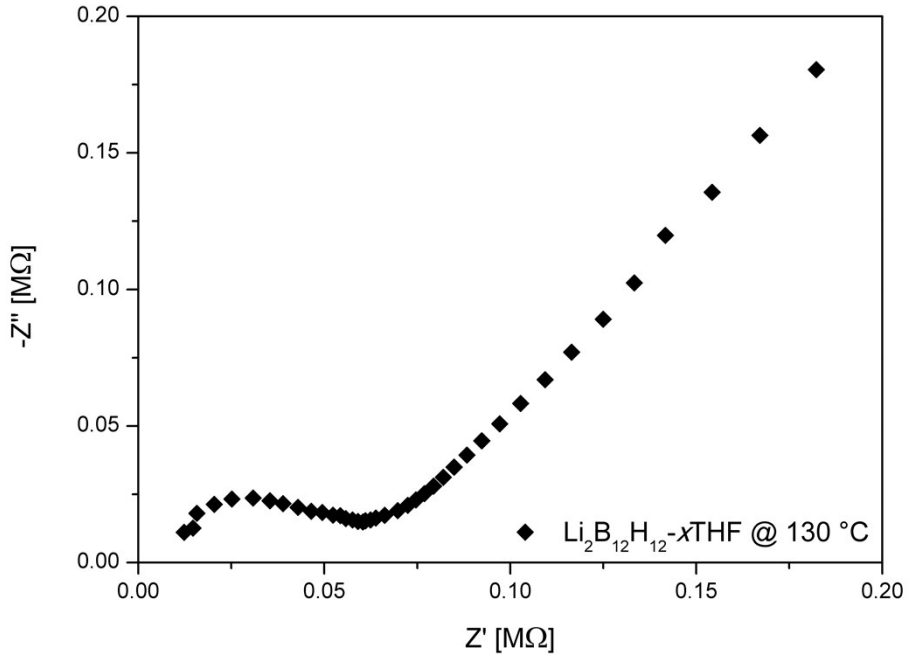

Figure S21. Nyquist plot of the molten $Li_2B_{12}H_{12}$-*x*THF sample at $T = 130$ °C.

References

1 Y. Yan, D. Rentsch, C. Battaglia and A. Remhof, *Dalton Trans.*, 2017, **46**, 12434–12437.
2 G. M. Sheldrick, *Acta Crystallogr. Sect. C Struct. Chem.*, 2015, **71**, 3–8.
3 G. M. Sheldrick, *Acta Crystallogr. A*, 2008, **64**, 112–122.
4 B. R. S. Hansen, K. T. Møller, M. Paskevicius, A.-C. Dippel, P. Walter, C. J. Webb, C. Pistidda, N. Bergemann, M. Dornheim, T. Klassen, J.-E. Jørgensen and T. R. Jensen, *J. Appl. Crystallogr.*, 2015, **48**, 1234–1241.
5 M. Paskevicius, M. B. Ley, D. A. Sheppard, T. R. Jensen and C. E. Buckley, *Phys. Chem. Chem. Phys.*, 2013, **15**, 19774–19789.
6 C. A. Dreiss, K. S. Jack and A. P. Parker, *J. Appl. Crystallogr.*, 2006, **39**, 32–38.
7 L. Fan, M. Degen, S. Bendle, N. Grupido and J. Ilavsky, *J. Phys. Conf. Ser.*, 2010, **247**, 012005.
8 B. R. S. Hansen, M. Paskevicius, M. Jørgensen and T. R. Jensen, *Chem. Mater.*, 2017, **29**, 3423–3430.
9 A. K. Mollner, P. A. Brooksby, J. S. Loring, I. Bako, G. Palinkas and W. R. Fawcett, *J. Phys. Chem. A*, 2004, **108**, 3344–3349.
10 J. E. Bertie and Z. Lan, *J. Phys. Chem. B*, 1997, **101**, 4111–4119.
11 K. M. Lange, K. F. Hodeck, U. Schade and E. F. Aziz, *J. Phys. Chem. B*, 2010, **114**, 16997–17001.